

# Low energy electron interactions with resveratrol and resorcinol: anion states and likely dissociation pathways

Ely G. F. de Miranda,<sup>\*,†</sup> Lucas M. Cornetta,<sup>\*,‡</sup> and Márcio T. do N. Varella<sup>\*,†</sup>

<sup>†</sup>*Instituto de Física, Universidade de São Paulo, Rua do Matão 1371, 05508-090, São Paulo, São Paulo, Brazil*

<sup>‡</sup>*Instituto de Física Gleb Wataghin, Universidade Estadual de Campinas, Rua Sérgio Buarque de Holanda, 777 - Cidade Universitária, Campinas, São Paulo, Brazil*

E-mail: ely.miranda@usp.br; lucascor@unicamp.br; mvarella@if.usp.br

## Abstract

We report a computational study of the anion states of the resveratrol (RV) and resorcinol (RS) molecules, also investigating dissociative electron attachment (DEA) pathways. RV has well known beneficial effects in human health, and its antioxidant activity was previously associated with DEA reactions producing  $H_2$ . Our calculations indicate a valence bound state ( $\pi_1^*$ ) and four resonances ( $\pi_2^*$  to  $\pi_5^*$ ) for that system. While the computed thermodynamical thresholds are compatible with DEA reactions producing  $H_2$  at 0 eV, the well known mechanism involving vibrational Feshbach resonances built on a dipole bound state should not be present in RV. Our results suggest that the shallow  $\pi_1^*$  valence bound state is expected to account for  $H_2$  elimination, probably involving  $\pi_1^*/\sigma_{OH}^*$  couplings along the vibration dynamics. The RS molecule is also an oxidant and a subunit of RV. Since two close-lying hydroxyl groups are found in the RS moiety, the  $H_2$ -elimination reaction in RV should take place at the RS site.

Our calculations point out a correspondence between the anion states of RV and RS, and even between the thresholds. Nevertheless, the absence of bound anion states in RS, indicated by our calculations, is expected to suppress the H<sub>2</sub>-formation channel at 0 eV. One is lead to conclude that the ethene and phenol subunits in RV stabilize the  $\pi_1^*$  state, thus switching on the DEA mechanism producing H<sub>2</sub>.

## Introduction

Life in our planet relies on two fundamental process: respiration and photosynthesis. They provide the means for the cellular energy production which is necessary for the living organisms.<sup>1</sup> Both processes are inseparably linked with the presence of electrons moving through biological matter.<sup>2</sup> This balance is fulfilled along electron transfer pathways, in particular the mitochondrial electron transport chains (ETCs).<sup>3</sup> However, reactive oxygen species (ROS), which are also produced along the mitochondrial ETC, are efficient oxidative substances capable of damaging the mitochondrial membranes, attacking DNA and causing mutations.<sup>4</sup> Molecular oxygen reduction generates the anionic superoxide,  $O_2 + e^- \rightarrow O_2^{\bullet -}$ , which can give rise to oxidative stress<sup>5</sup> leading to pathologies such as cardiovascular diseases, Alzheimer's and Parkinson's.<sup>6,7</sup> Nonetheless, ROS can also be beneficial to the cell, e.g., by producing oxidative damage to pathologies and taking part in cellular signaling.<sup>5</sup> Protective mechanisms that neutralize ROS are linked with the generation of native antioxidants or enzymatic activity. Oxireductive balance perturbations in mitochondrial intermembrane space are therefore believed to trigger significant cellular damage.<sup>8</sup>

Polyphenolic antioxidants, such as flavonoids and spinochromes, are good electron acceptors and can interact with electrons under reductive conditions in cells.<sup>9</sup> Dissociative electron

attachment (DEA) to multiple OH-substituted aromatic compounds has been found to produce neutral  $H_2$ ,<sup>9</sup> which is an antioxidant species used clinically.<sup>10</sup> These facts suggest that the antioxidant activity of polyphenolic compounds could be related to the electron-induced production of molecular hydrogen. The xenobiotic antioxidant compounds could be reduced in the mitochondrial intermembrane space by charge leaking from the ETC. The reduction can be viewed as the formation of transient negative ions (TNIs), also called resonances, that can initiate DEA reactions producing  $H_2$  among other species. These mechanisms have been proposed to underlie the antioxidant activity of the polyphenolic compound resveratrol (RV)<sup>11</sup> and also the antipsoriatic activity of anthralin.<sup>12</sup>

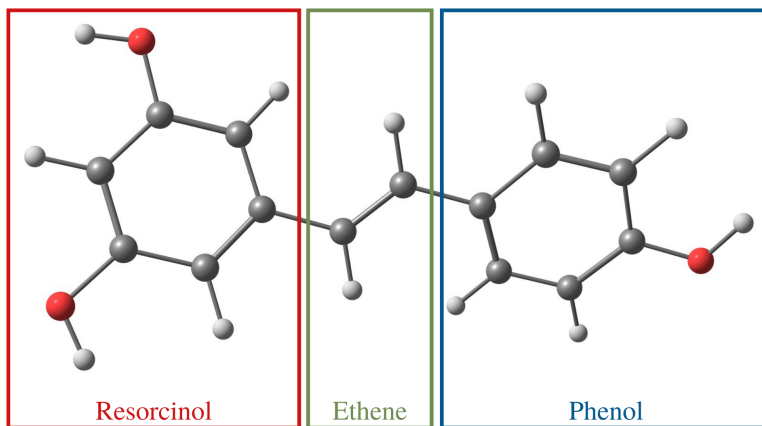


Figure 1: Structure of the resveratrol molecule, with the oxygen atoms indicated in red, carbon in gray, and hydrogen in white. The resorcinol, ethene and phenol subunits are highlighted.

The RV molecule (3,5,4'-trihydroxystilbene, shown in Fig. 1) is a naturally occurring plant phytoalexin and a constituent of red wine. It is known for its strong antioxidant activity<sup>13</sup> and produces beneficial effects in human health by preventing a variety of illnesses, such as cancer, cardiovascular malfunction, neurodegenerative diseases, inflammation, and atherosclerosis.<sup>13</sup> The mechanisms underlying those beneficial effects are not yet clear. Since

H and H<sub>2</sub> can be produced by DEA to RV, we presently investigate the TNIs employing electron scattering calculations, and we also infer the possible dissociation pathways. A major difficulty to model the transient anion states of RV is the computational effort arising from the system size and lack of symmetry elements. The RV molecule has 29 atoms and can be considered large for scattering calculations. However, RV can be decomposed into resorcinol (RS), ethene and phenol (Ph) subunits, as indicated in Fig. 1. The smaller subunits have been the subject of previous studies,<sup>14,15</sup> so we presently consider RS, which is also an antioxidant.<sup>16,17</sup> In view of the two hydroxyl groups lying at meta positions with respect to each other in RS, H<sub>2</sub>-elimination reactions in RV are likely to take place at the RS moiety. To this extent, the smaller RS molecule could be a more suitable prototype for the DEA reaction producing molecular hydrogen, justifying the study of both the RS and RV molecules. We therefore investigate the bound and transient anion states of those molecules, as well as the thermodynamical thresholds, in order to infer the DEA mechanisms for H- and H<sub>2</sub>-elimination reactions.

This paper is organized as follows. In Sec. II we present the theoretical and computational methods for scattering calculations (Schwinger Multichannel Method with Pseudopotentials) employed for the anions characterizations. In Sec. III and IV we present the calculations and discuss our findings. Finally, the conclusions are summarized in Sec. V.

## Computational Procedures

All scattering calculations were performed in the fixed-nuclei approximation. Equilibrium geometries and vibrational analysis for the neutral molecules were performed with density

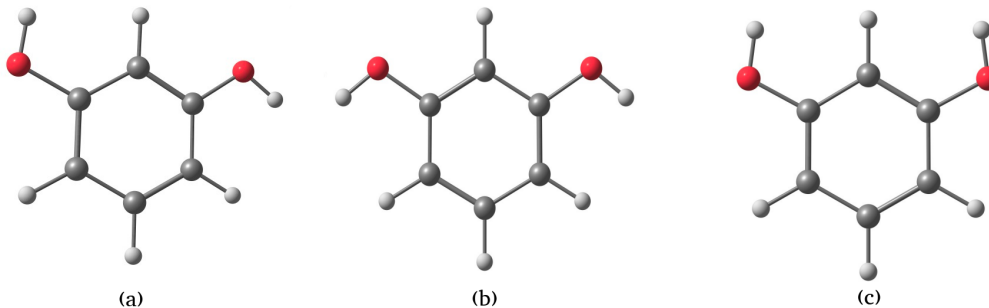


Figure 2: Planar conformers of the resorcinol molecule, labeled (a) to (c). The oxygen atoms are indicated in red, carbon in gray and hydrogen in white.

functional theory (DFT), employing the  $\omega$ B97XD functional and the 6-311++G(d,p) basis set, as implemented in the Gaussian09 package.<sup>18</sup> Three planar conformers were identified for the RS molecule, differing by the orientation of the hydroxyl groups, as shown in Fig. 2. The conformers (b) and (c) belong to the  $C_{2v}$  symmetry point group, while the conformer (a) belongs to the  $C_s$  group. Based on the free energies at room temperature ( $k_B T \approx 26$  meV), we assign the conformer (b) as the most stable one, lying 2 meV and 28 meV below the (a) and (c) forms, respectively. Therefore, an admixture of the three conformers should be present in gas-phase experiments justifying scattering calculations for all of them. In contrast to the small differences in the free energy values, the dipole moment magnitudes are significantly affected by the orientation of the hydroxyl groups. We obtained  $\mu = 1.4$  D for the optimal structure (a), against  $\mu = 2.5$  D and  $\mu = 2.3$  D for conformers (b) and (c), respectively.

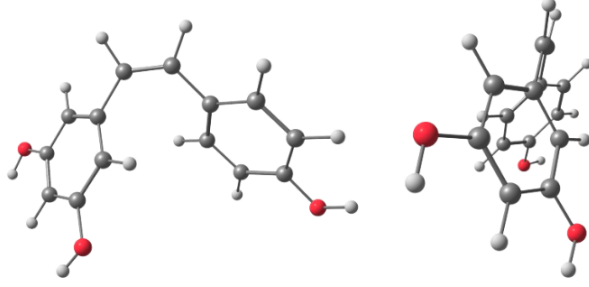
For the RV molecule, the existence of cis (c-RV) and trans (t-RV) isomers deserves a closer look. The relative ground state energies of the RV isomers, also calculated with the  $\omega$ B97XD/6-311++G(d,p) method, indicate that the t-RV isomer is significantly more stable than the cis counterpart, by 0.3 eV. While the geometries of the cis and trans isomers are

shown in Fig. 3, we no further consider the *cis* form in view of the negligible Boltzmann populations. The geometry of the *t*-RV isomer was somewhat sensitive to the choice of the exchange-correlation functional. The  $\omega$ B97XD/6-311++G(d,p) calculations predict a torsion angle between the aromatic rings around 15 degrees (see Tab. S1). However, exploratory optimizations performed with the B3LYP/6-311++G(d,p) method indicate a smaller angle, around 4 degrees, in agreement with previously reported DFT/B3LYP results.<sup>11</sup> Since dispersion interactions are accounted for in the  $\omega$ B97XD functional, although not in B3LYP, the discrepancy in the torsion angle suggests that the interaction between the unsaturated rings would not be accurately described without dispersion corrections.<sup>19,20</sup> For the RS conformers, not having inter-ring  $\pi$ - $\pi$  interactions, the B3LYP and  $\omega$ B97XD functionals predict similar structures.

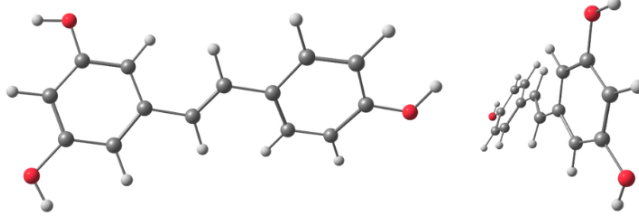
Despite the deviation from planarity arising from the torsion angle, the scattering calculations employed a planarized geometry of the *t*-RV isomer, referred to as *p*-RV (also computed with the  $\omega$ B97XD/6-311++G(d,p) method, see Fig. 3). Previous scattering studies of nucleobases<sup>21-23</sup> used a similar procedure, since the planar structures allow for symmetry decomposition which reduces the computational effort. In addition, the signatures of the shape resonances become more evident in the symmetry-decomposed calculated cross sections. We estimated errors around 0.1eV between *t*- and *p*-RV resonance positions employing empirically corrected virtual orbital energies, according to Scheer and Burrow.<sup>24</sup>

The scattering cross sections were computed with the parallel version of the Schwinger multichannel method implemented with the Bachelet-Hamann-Schlüter (BHS) pseudo potentials (SMCPP).<sup>25,26</sup> The method was recently reviewed,<sup>27</sup> so we briefly outline a few

cis-RV



trans-RV



planar-RV

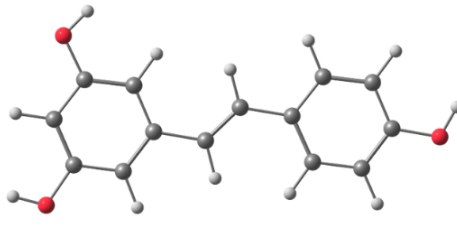


Figure 3: Structures of the RV molecule computed with the  $\omega$ B97XD/6-311++G(d,p) method (front and side views). The oxygen atoms are represented in red color, carbon in gray, and hydrogen in white.

relevant aspects. The scattering electronic wave function is given by

$$\left| \Psi_{\mathbf{k}_i}^{(\pm)} \right\rangle = \sum_{\mu} c_{\mu}^{(\pm)}(\mathbf{k}_i) |\chi_{\mu}\rangle, \quad (1)$$

where  $\mathbf{k}_i$  denotes the wave vector of the incident electron and  $+$ ( $-$ ) stands for the boundary condition associated with outgoing (incoming) spherical waves.<sup>28</sup> The method uses square-integrable functions to build the trial set  $\{\chi_{\mu}\}$ , which is very convenient from the computational point of view. The basis vectors  $|\chi_{\mu}\rangle$  are referred to as configuration state functions

(CSFs), and correspond to spin-adapted  $(N + 1)$ -particle Slater determinants built on the closed-shell ground state of the neutral target, comprising  $N$  electrons. The latter reference state is described at the restricted Hartree-Fock (RHF) level, employing sets of Cartesian Gaussian basis functions. The  $5s5p2d$  basis sets described by Bettega *et al*<sup>26,29</sup> were used for the carbon and oxygen atoms, while the  $4s$  basis set reported by Dunning<sup>30</sup> was used for the hydrogens, amounting to a total of 274 basis functions for each RS structure and 580 for the p-RV structure. The RHF calculations were performed with the GAMESS package.<sup>31</sup>

The scattering calculations were restricted to the elastic channel, which is a reasonable approximation for electron energies below the excitation threshold. Two models were explored to construct the CSF space. In the static-exchange (SE) approximation, the target is kept frozen in the ground state  $|\Phi_0\rangle$ , while the unoccupied (virtual) orbitals are used as scattering orbitals  $|\phi_m\rangle$ , i.e.,  $|\chi_m\rangle = \mathcal{A}_{N+1} |\Phi_0\rangle \otimes |\phi_m\rangle$ , where  $\mathcal{A}_{N+1}$  is the anti-symmetrization operator. This approximation does not recover the response of the target electrons to the incoming electron. Even though the SE approach retrieves the physics of shape resonances, at lower energies the dynamical response of the target electrons, referred to as correlation-polarization effects, should be accounted for. In the static-exchange plus polarization (SEP) approximation, virtual excitations of the target are allowed, so the CSF space is augmented with configurations of the type  $|\chi_{im}\rangle = \mathcal{A}_{N+1} |\Phi_i\rangle \otimes |\phi_m\rangle$ , in which  $|\Phi_i\rangle$  represents a singly excitation of the target and  $|\phi_m\rangle$  is a scattering orbital. In this approximation, long-range polarization (induced dipole moment) and short-range correlation are taken into account. The SEP functions require the choice of three orbitals, two of which are associated with the excitation of the target (hole and particle) and the third being the scattering orbital. The CSF space is build according to the energy criterion proposed by Kossoski and Bettega.<sup>32</sup>



All single-particle orbitals whose energy eigenvalues satisfy  $\epsilon_{\text{scat}} + \epsilon_{\text{part}} - \epsilon_{\text{hole}} < \Delta$ , are taken into account, where  $\epsilon_{\text{scat}}$ ,  $\epsilon_{\text{part}}$ , and  $\epsilon_{\text{hole}}$  are the energies of the scattering, particle, and hole orbitals, respectively, while  $\Delta$  is a cutoff. Finally, modified virtual orbitals (MVOs)<sup>33</sup> were used as particle and scattering orbitals. They were generated from cationic Fock operators with charge +6 for RS and +8 for RV.

The integral cross sections (ICSs) of a-RS and p-RV were decomposed into the  $A'$  and  $A''$  components of the  $C_S$  group, while for the b-RS and c-RS the ICSs are decomposed into the four components of the  $C_{2v}$  group, namely  $A_1$ ,  $A_2$ ,  $B_1$  and  $B_2$ . In the SEP approximation for a-RS, we employed  $\Delta = -0.95$  Hartree for the  $A'$  and  $A''$  components, generating 15405 and 15228 configurations. Similarly, for b-RS (c-RS), we employed  $\Delta = -0.85$  Hartree for the  $A_1$  component, resulting in 9978 (10053) configurations, and  $\Delta = -1.00$  Hartree for  $A_2$ ,  $B_1$  and  $B_2$  components, resulting in 6619 (6633), 6682 (6724) and 6654 (6654) configurations, respectively. For the case of p-RV, only the  $A''$  component was considered, since we do not expect resonance signatures in the  $A'$  ICS component. In this case, we employed  $\Delta = -0.95$  Hartree resulting in 17969 CFSs.

While only elastic collisions were taken into account, some insight into the inelastic channels can be gained from bound state calculations. The lowest lying excited states of the neutral RS molecule were explored with the CASPT2 method.<sup>34</sup> These calculations were performed with the OpenMOLCAS software,<sup>35</sup> and the active space is described in the supplementary information (SI). Finally, DEA reaction thresholds were estimated with the composite G4(MP2) method,<sup>36</sup> as implemented in the Gaussian09 package. The thresholds were estimated as the difference between the G4(MP2) energies of products, including the anionic fragment, with respect to the energy of the neutral reactant (see Sec. IV).

# Results

As expected, only  $\pi^*$  resonances have clear signatures in the calculated ICSs, for both RV and RS. The corresponding peaks appear in the  $A_2$  and  $B_1$  components of  $C_{2v}$  molecules (b- and c-RS), while in the  $A''$  component of  $C_S$  molecules (a-RS and p-RV). It is worth noting that  $C_S$  is a subgroup of  $C_{2v}$ , so the sum of the  $A_2$  and  $B_1$  components correspond to  $A''$ . In the upper panel of Fig. 4, we show the SEP-level ICSs obtained for a-RS ( $A''$  component), as well as b-RS and c-RS ( $A_2+B_1$  components). We observed three  $\pi^*$  shape resonances for all geometries. These are labeled  $\pi_1^*$  to  $\pi_3^*$ , in order of increasing energy, according to the virtual orbitals that accommodate the additional electron. Respectively for a-, b- and c-RS, the anion states are located at 0.75, 0.84 and 0.78 eV ( $\pi_1^*$ ); 1.21, 1.33 and 1.34 eV ( $\pi_2^*$ ); and 5.70, 5.79 and 5.78 eV ( $\pi_3^*$ ). The positions obtained for the three structures are in good agreement among them. The excitation threshold of the first excited state of the target molecule was estimated as  $\approx 3.9$  eV for all isomers, indicating that the  $\pi_3^*$  resonance might have a mixed shape and core-excited character.

The SMCPP method allows for the diagonalization of the scattering Hamiltonian represented in the square-integrable CSF basis. This procedure generates a set of pseudo-states, since the actual spectrum is not discrete, but it provides insight into the resonance orbitals. The orbital plots shown in Fig. 5 were obtained from the SEP-approximation pseudo-eigenstates, although projecting them on the SE subspace. The properly renormalized projections of the eigenstates can be recast as linear combinations of the MVOs, which represent the resonant orbital (occupied by the attached projectile). Even though we only show orbitals for the c-RS structure, similar results were obtained for the other RS isomers.

The calculated positions and widths of the resonance states are summarized in Tab. 1. The SEP-approximation results for the RS structures are generally in good agreement, except for the width of the  $\pi_1^*$  anion state. The 50-meV difference can nevertheless be viewed as small in absolute value. The widths were obtained from standard local-approximation fits of Breit-Wigner profiles to the calculated eigenphase sums, so the origin of the discrepancy is unclear.

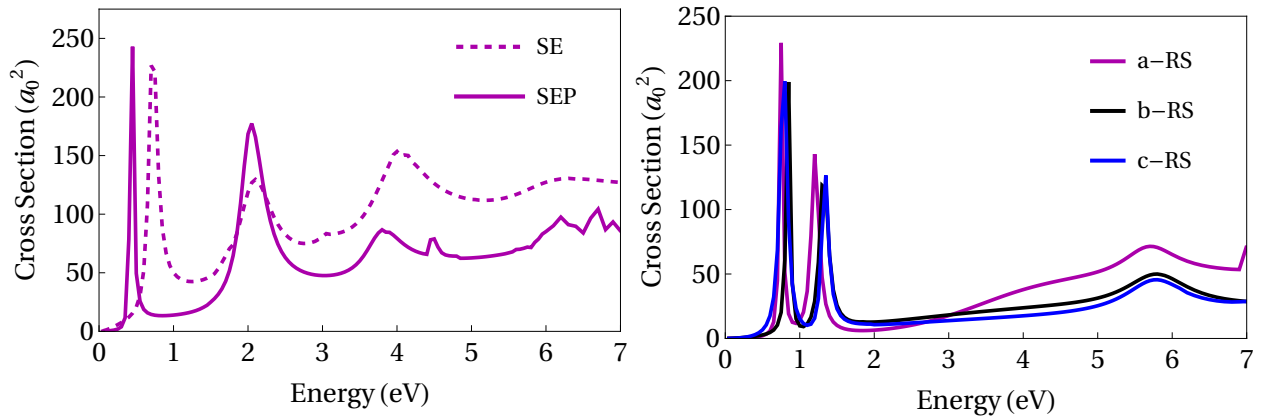


Figure 4: Left panel:  $A''$  integral cross section of neutral p-RV calculated in SE - dashed line - and SEP - filled line - approximations; Right panel:  $A_2$  plus  $B_1$  (for b and c-RS) and  $A''$  (for a-RS) integral cross section for elastic electron scattering by the a (magenta line), b (black line) and c (blue line) structures of RS.

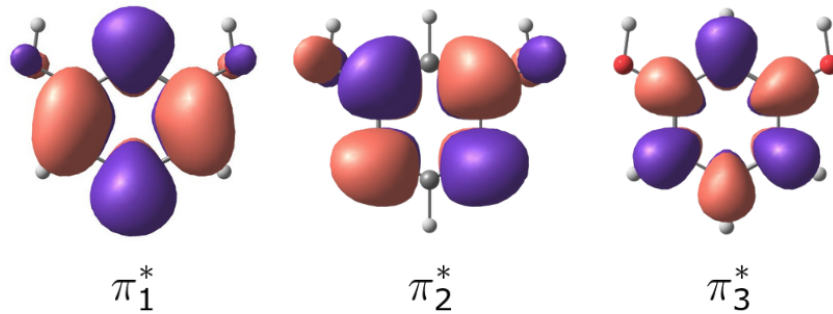


Figure 5:  $\pi^*$  type orbitals of RS obtained from the pseudo-eigenstates of the scattering Hamiltonian. The orbitals are linear combinations of the MVOs employed in the scattering calculations.

The lower panel of Fig. 4 shows the  $A''$  component of the ICS for p-RV. The SE calcu-

Table 1: Resonance positions and widths (given in parenthesis), in units of eV, for a-, b-, and c-RS, as well as p-RV. SEP results are reported for RS, while SE and SEP for RV. The negative energy value indicates a bound state of the anion.

System	$\pi_1^*$	$\pi_2^*$	$\pi_3^*$	$\pi_4^*$	$\pi_5^*$
a-RS	0.75 (0.05)	1.21 (0.12)	5.70 (0.91)	-	-
b-RS	0.84 (0.06)	1.33 (0.13)	5.79 (1.02)	-	-
c-RS	0.78 (0.11)	1.34 (0.11)	5.78 (1.02)	-	-
p-RV (SE)	0.72 (0.13)	2.09 (0.54)	4.02 (0.91)	6.10 (2.12)	10.24 (2.46)
p-RV (SEP)	-0.07	0.44 (0.05)	2.05 (0.39)	2.05 (0.39)	3.81 (0.56)

lations point out five  $\pi^*$  shape resonances around 0.72 eV ( $\pi_1^*$ ), 2.09 eV ( $\pi_2^*$ ), 4.02 eV ( $\pi_3^*$ ), 6.10 eV ( $\pi_4^*$ ) and 10.24 eV ( $\pi_5^*$ ) (see also Tab. 1). The interpretation of the SEP results for this system turned out to be more difficult, since we only identified three  $\pi^*$  shape resonances, at 0.44 eV, 2.05 eV and 3.81 eV. The SEP spectrum could be clarified by inspecting the pseudo-eigenstates of the scattering Hamiltonian, as described above. The lowest-lying  $\pi_1^*$  state becomes bound with respect to the neutral molecule by 70 meV, in consistency with previous results.<sup>11</sup> The 0.44-eV peak can be assigned to the  $\pi_2^*$  resonance, while the  $\pi_3^*$  and  $\pi_4^*$  states merge into a single peak around 2.05 eV. The overlap between these resonances explain the apparently absent peak in the SEP results. Lastly, the signature of the  $\pi_5^*$  state, expected to have mixed character, is found around 3.8 eV. In general, a balanced description of polarization effects among several resonances belonging to the same irreducible representation is a challenging task in SEP calculations. Since there are five anion states in the  $A''$  symmetry component of RV, our SEP results might not be properly balanced. It should be clear that going beyond the SEP approximation for a system as large as RV would not be a trivial computational task. The  $\pi^*$  orbital plots obtained from the SEP-approximation pseudo eigenstates projected on the SE space are shown in Fig. 6.

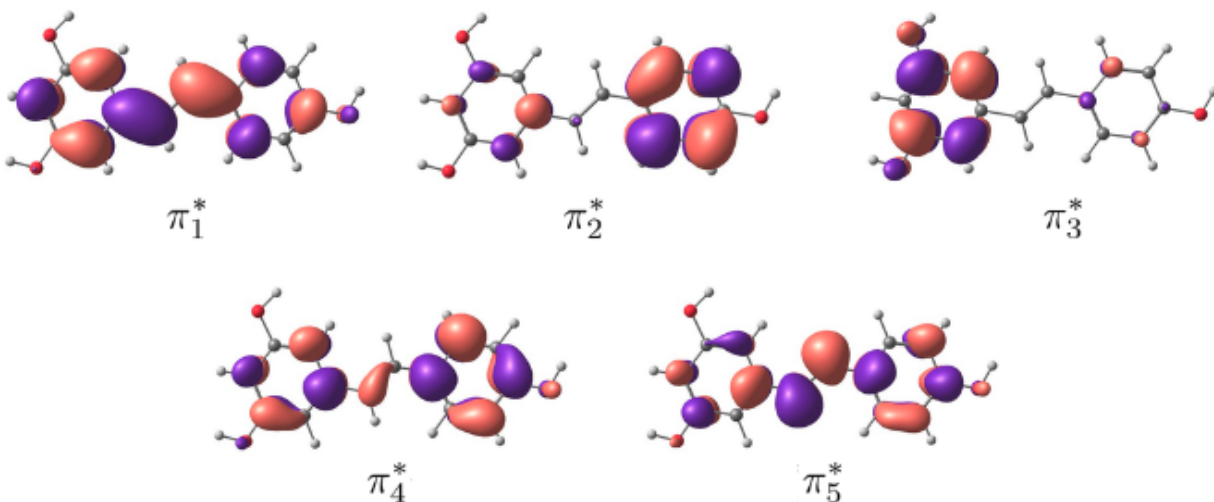


Figure 6: p-RV  $\pi^*$  type orbitals obtained from the pseudo-eigenstates of the scattering Hamiltonian. The orbitals are linear combinations of the MVOs employed in the scattering calculations.

## Discussion

DEA to RV was investigated experimentally.<sup>8,11</sup> While the target molecules were evaporated at 170° C, and the collision cell kept at 180° C to avoid condensation, the c-RV isomer is not expected to have a significant Boltzmann population, as discussed above. The main fragments observed in the energy- and mass-resolved measurements are summarized in Tab. 2, along with the peak energies and relative intensities. The calculated energy of the  $\pi_2^*$  state, 0.44 eV, is compatible with the DEA peak for the elimination of two hydrogens (0.6 eV). The nearly degenerate resonances,  $\pi_3^*$  and  $\pi_4^*$ , are expected to give rise to the most intense DEA signal (1.2 eV), corresponding to the H-elimination reaction. The disagreement in energy is another indication that our scattering calculations overestimate the resonances positions (2.0 eV). Finally, the DEA peaks around 4 eV are compatible with the  $\pi_5^*$  resonance, which was predicted at 3.8 eV (SMCPP). In this case the SMCPP result seems in better agreement

with the data, but it could be to some extent fortuitous, since core-excited anion states may account for the signal around 4.0 eV, at least partly. The abstraction of H atoms mediated by  $\pi^*$  resonances should also involve  $\sigma^*$  anion states with anti-bonding character on the polar OH groups. Those resonances typically do not have clear signatures in the scattering cross sections,<sup>25,37,38</sup> although indirect evidence can be provided by virtual orbitals calculated with compact basis sets. As shown in Fig. 7, we could find anti-bonding virtual orbitals with  $\sigma_{\text{OH}}^*$  character and similar amplitudes in the Ph and RS subunits of the RV molecule.

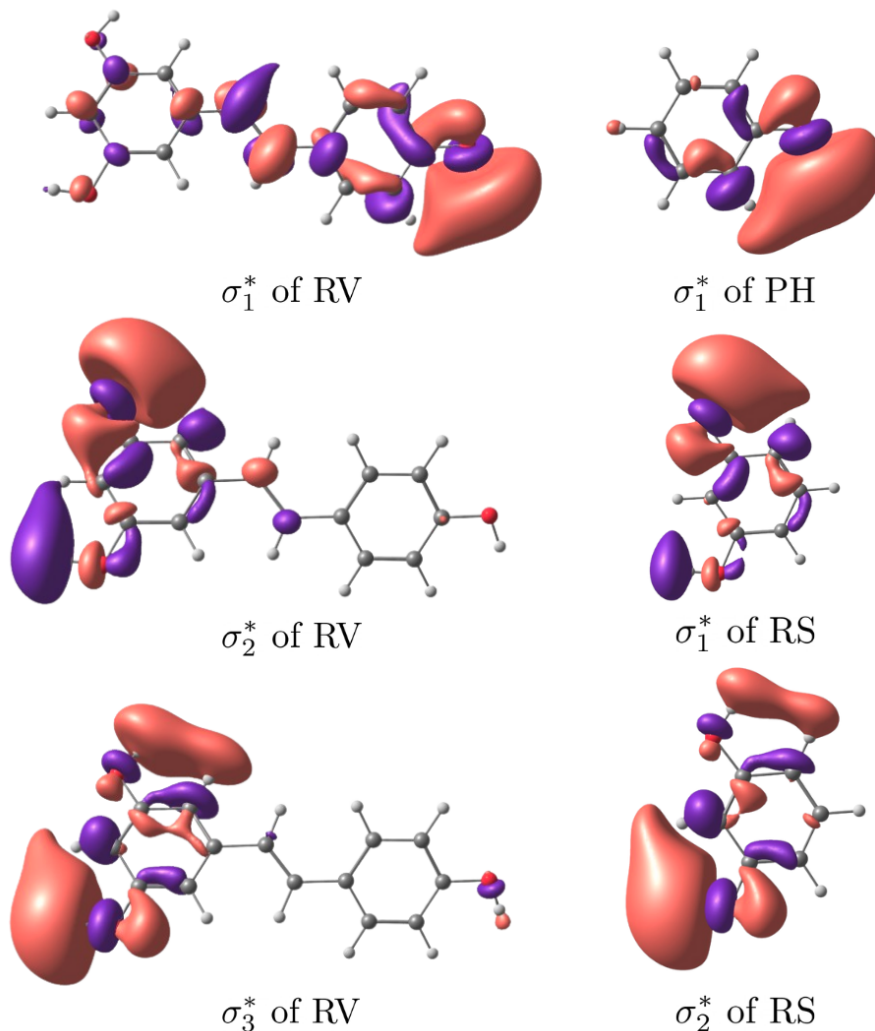


Figure 7:  $\sigma^*$  virtual orbitals obtained with the  $\omega\text{B97XD}/6\text{-}31\text{G}^*$  for the RV, RS and Ph molecules.

Table 2: Anion fragments observed in DEA experiments.<sup>11</sup> The fragments, peak energies (in eV) and relative intensities are shown (the asterisk indicates a low intensity).

Fragment	Energy	Intensity
M <sup>-</sup>	0.0	45
[M-H] <sup>-</sup>	1.2	100
	4.3	24
[M-2H] <sup>-</sup>	0.0	17
	0.6	*
[M-3H] <sup>-</sup>	4.5	0.8
	9.5	1.3
[M-(CH) <sub>2</sub> OH] <sup>-</sup>	8.7	0.8

Turning attention to the DEA signals at 0 eV, one should remind that the dipole moment of the RV molecule can exceed 3.0 D in case the hydroxyl groups in the RS subunit are properly aligned, as shown in Fig. 8. We employed the aug-cc-pVDZ basis set augmented with a 6s6p set of diffuse functions, as suggested by Skurski *et al.*,<sup>39</sup> to survey dipole-supported states in the RV conformers. We could only converge a DBS for the most strongly polar form ( $\mu = 3.3$  D). The binding energy obtained at the MP2 level was very small, below 1 meV. Even if the DBS exists at all, we believe the well known mechanism for H elimination,<sup>40</sup> initiated by vibrational Feshbach resonances (VFRs) built on a DBS, would not account for the 0 eV signal in RV. According to our  $\omega$ B97XD/6-311++G(d,p) calculations, the ground state of neutral RV has three OH stretch modes with energies close to 3920 cm<sup>-1</sup> (0.49 eV). In view of the nearly zero binding energy of the DBS, the  $\nu_{\text{OH}} = 1$  VFRs would lie significantly above the observed DEA peak, around 0.5 eV. In addition, the orientation of the dipole vector in the most strongly polar conformer favors H elimination from the Ph subunit, such that the formation of molecular hydrogen would be unlikely. The direction of the dipole

moment favors  $\text{H}_2$  elimination in a less polar conformation ( $\mu = 2.3$  D, see Fig. 8), but we could not obtain a DBS for this conformer.

As mentioned above, the diagonalization of the scattering Hamiltonian indicates a bound  $\pi_1^*$  state for the p-RV geometry. This result is confirmed by  $\omega\text{B97XD}/6\text{-}311\text{++G(d,p)}$  calculations for t-RV (binding energy of 50 meV), although not by the  $\text{B3LYP}/6\text{-}311\text{++G(d,p)}$  calculations. Since the DEA data at 0 eV is compatible with the existence of a bound anion state, we believe the shallow  $\pi_1^*$  state should account for the low-energy DEA signals. The binding energy ( $\approx 50$  meV) is rather close to the thermal energy under experimental conditions ( $k_B T = 39$  meV), such that VFRs at 0 eV can arise from low-energy vibrational modes, ranging from  $\sim 0$  to  $\sim 50$  meV. Relaxation of the  $\pi_1^*$  state is favored by the dense vibrational spectrum, in consistency with the observation of the parent  $\text{M}^-$  anion at 0 eV. Even though the pathway for  $\text{H}_2$  elimination is not evident, it should involve  $\pi_1^*/\sigma_{\text{OH}}^*$  couplings along the vibration dynamics.

The calculated reaction thresholds for the H- and  $\text{H}_2$ -elimination channels are shown in Fig. 9 for zero temperature (black) and  $T = 453.15$  K (red), which is consistent with the experimental condition. We show results for the a-RS conformer (results are similar for the other conformers), Ph and RV. Our calculations corroborate that  $\text{H}_2$  elimination at low energies should not take place at the Ph subunit, since the dissociation of the CH bonds is energetically less favorable compared to the polar OH bonds. On the other hand, the thresholds for H abstraction from Ph and a-RS are similar (though not discussed here, our results are consistent with the DEA data for Ph<sup>14,41,42</sup>). The present threshold estimates are generally in agreement with previous calculations.<sup>11</sup>

The formation of  $\text{H}_2$  from RV, along with the meta-benzoquinone (MBQ) anion, has a



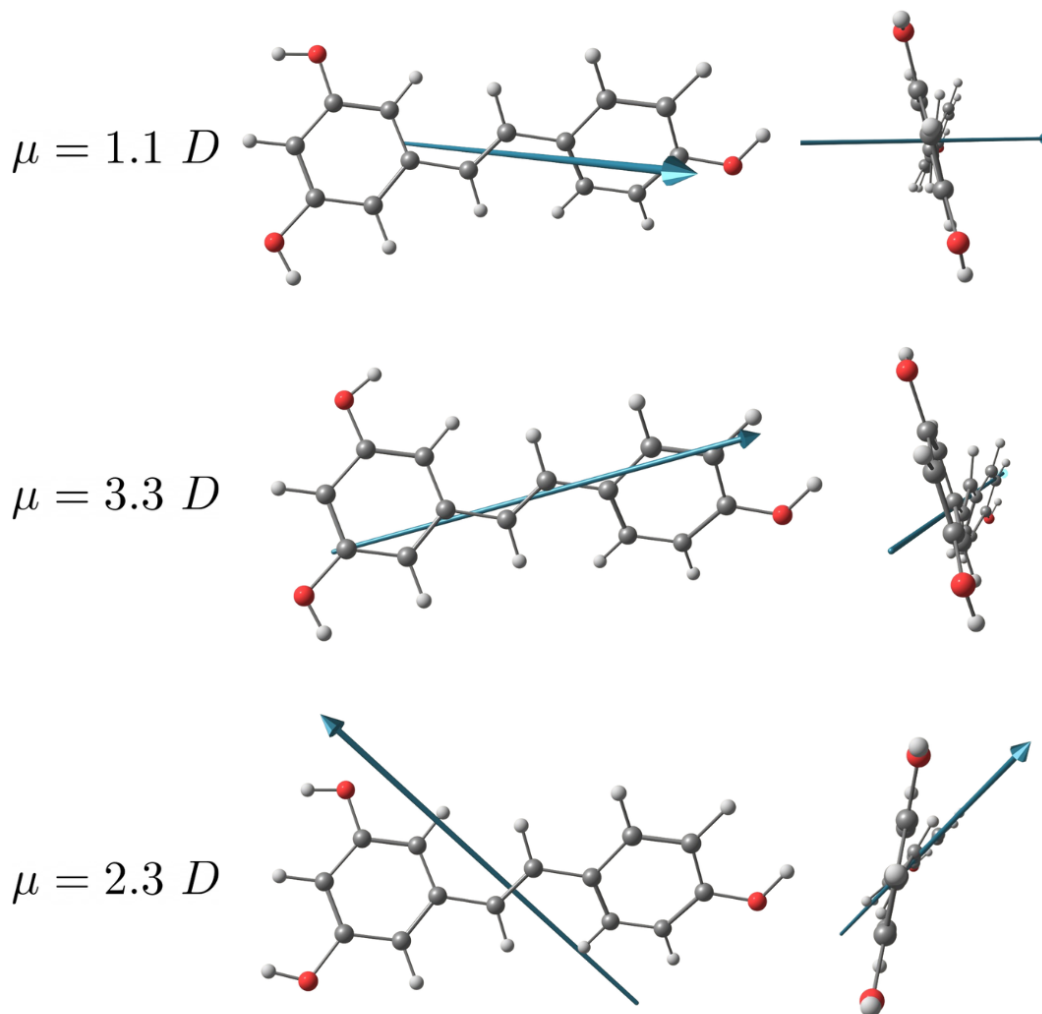


Figure 8: Dipole moment vector and magnitude of the three RV isomers calculated with  $\omega$ B97XD/6-311++G(d,p).

nearly zero threshold at 0 K, and the reaction becomes exothermic at higher temperatures. This is of course consistent with the formation  $H_2$  at 0 eV. The calculated thresholds for H abstraction at 453 K are 0.3 eV (Ph subunit) and 0.5 eV (RS subunit). These estimates are also consistent with the observation of the  $[M-H]^-$  fragment at 1.2 eV although not at 0 eV. Other fragments were observed at considerably higher energies (see Tab. 2), so they cannot be interpreted based on our calculations.

As stated above, one of the goals of our work was to investigate if the smaller RS molecule

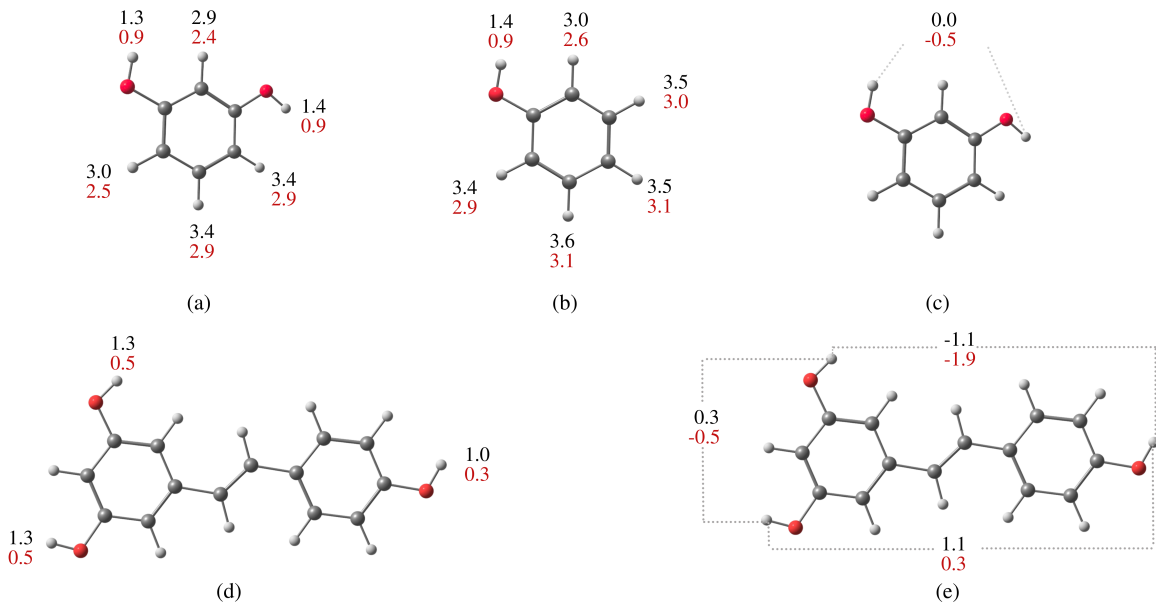


Figure 9: Free energy dissociation thresholds (in units of eV) obtained for: (a) H abstraction from a-RS ( $\text{a-RS} + e^- \rightarrow [(\text{a})\text{-RS} - \text{H}]^- + \text{H}^\bullet$ ); (b) H abstraction from Ph ( $\text{Ph} + e^- \rightarrow [\text{Ph} - \text{H}]^- + \text{H}$ ); (c) H<sub>2</sub> abstraction from a-RS ( $\text{a-RS} + e^- \rightarrow \text{MBQ}^{\bullet-} + \text{H}_2$ ); (d) H abstraction from p-RV ( $\text{p-RV} + e^- \rightarrow [\text{p-RV} - \text{H}]^- + \text{H}^\bullet$ ) and; (e) H<sub>2</sub> abstraction from p-RV ( $\text{p-RV} + e^- \rightarrow [\text{p-RV} - 2\text{H}]^{\bullet-} + \text{H}_2$ ). The black and red numbers indicate, respectively, the thresholds at  $T = 0$  and  $T = 453.15$  K. The sites where the abstraction reactions take place are indicated by the position of the energy values in each panel.

would be a prototype for the H<sub>2</sub>-elimination reactions in RV. Molecular dynamics and reaction paths simulations would be considerably less demanding for the smaller system, apart from the advantages discussed above for the scattering computations (symmetry decomposition, dimension of CSF space and polarization balance). While the formation of H<sub>2</sub> would also be exothermic in RS, the reaction should be suppressed by the absence of bound anion states. As stated above, the dipole moment magnitudes range from 1.4 D to 2.5 D, depending on the isomer, and our calculations do not indicate a DBS for RS (if the DBS exists at all, it should be very shallow). In addition, the  $\pi_1^*$  state, which is bound in RV, becomes a resonance in RS, lying around 0.7 eV. Since there are not bound anion states, the observation of  $[\text{M}-2\text{H}]^-$  fragments at 0 eV is not expected for RS. Our results are not in

disagreement with the known antioxidant properties of RS, since mechanisms not based on DEA have been pointed out.<sup>17</sup> The differences between RV and RS actually suggest that the ethene and Ph subunits of play a relevant role in the H<sub>2</sub>-elimination reaction, although an indirect one. Those subunits switch on the H<sub>2</sub>-elimination mechanism in RV, to the extent that they stabilize the  $\pi_1^*$  state.

## Conclusions

We reported a theoretical investigation of the low-energy anion states of the polyphenolic compound RV. This is a challenging system for electron scattering calculations in view of its size and low symmetry. Even though description of correlation-polarization effects is not well balanced in our SEP results, our study provides a consistent interpretation of the previously reported DEA measurements. In addition to four shape resonances, our results point out a shallow valence bound state  $\pi_1^*$ . This anion state, along with the computed dissociation thresholds, supports that H<sub>2</sub> elimination at 0 eV would be initiated by  $\pi_1^*/\sigma_{\text{OH}}^*$  couplings. Since we could only converge a very shallow DBS for RV, we do not believe that H elimination at 0 eV is initiated by vibrational Feshbach resonances (VFRs) built on a DBS. The  $\pi_1^*$  state is also responsible for the formation of the parent M<sup>-</sup> ion, also observed at 0 eV. The H-elimination reaction observed around 1.2 eV is triggered by two nearly degenerate shape resonances,  $\pi_3^*$  and  $\pi_4^*$ .

We also investigated the RS subunit, which could be a less computationally expensive prototype for the production of H<sub>2</sub>, a reaction that could account for the antioxidant activity of RV, at least partly. We obtained two  $\pi^*$  shape resonances and a mixed-character resonance

from SEP-level scattering calculations. There is a correspondence between the anion states of RV and RS, and even between the dissociation thresholds. However, the absence of bound anion states for the RS molecule is expected to suppress the H<sub>2</sub>-formation channel at 0 eV. Our calculations therefore unveil the indirect part played by the ethene and Ph moieties of RV. They switch on the H<sub>2</sub>-elimination mechanism initiated by  $\pi_1^*/\sigma_{\text{OH}}^*$  couplings, since they stabilize the  $\pi_1^*$  state.

## Acknowledgments

E. G. F. M. acknowledges financial support from São Paulo Research Foundation (FAPESP), under grants No. 2021/09837-7, Brazilian National Council for Scientific and Technological Development (CNPq), under grant No. 131628/2019-4. L. M. C. acknowledges financial support from FAPESP, under grants No. 2020/04822-9 and No. 2021/06527-7. M. T. do N. V. also acknowledges financial support (CNPq) (grant No. 304571/2018-0) and FAPESP (grant No.2020/16155-7). The calculations were partly performed with HPC resources from STI, University of São Paulo.

## References

- (1) Metzler, D. The chemical reactions of living cells. *Biochemistry* **1977**, 517–558.
- (2) Ahmad, M.; Wolberg, A.; Kahwaji, C. I. Biochemistry, electron transport chain. **2018**,
- (3) Pelster, L. N.; Minter, S. D. Mitochondrial inner membrane biomimic for the investigation of electron transport chain supercomplex bioelectrocatalysis. *Acs Catalysis* **2016**, 6, 4995–4999.

- (4) Costa, R.; Romagna, C. D.; Pereira, J.; Souza-Pinto, N. C. The role of mitochondrial DNA damage in the cytotoxicity of reactive oxygen species. *Journal of bioenergetics and biomembranes* **2011**, *43*, 25–29.
- (5) Murphy, M. P. How mitochondria produce reactive oxygen species. *Biochemical journal* **2008**, *417*, 1–13.
- (6) Koopman, W. J.; Willems, P. H.; Smeitink, J. A. Monogenic mitochondrial disorders. *New England Journal of Medicine* **2012**, *366*, 1132–1141.
- (7) Andreyev, A. Y.; Kushnareva, Y. E.; Starkov, A. Mitochondrial metabolism of reactive oxygen species. *Biochemistry (Moscow)* **2005**, *70*, 200–214.
- (8) Pshenichnyuk, S. A.; Modelli, A.; Komolov, A. S. Interconnections between dissociative electron attachment and electron-driven biological processes. *International Reviews in Physical Chemistry* **2018**, *37*, 125–170.
- (9) Modelli, A.; Pshenichnyuk, S. A. Gas-phase dissociative electron attachment to flavonoids and possible similarities to their metabolic pathways. *Physical Chemistry Chemical Physics* **2013**, *15*, 1588–1600.
- (10) Ohsawa, I.; Ishikawa, M.; Takahashi, K.; Watanabe, M.; Nishimaki, K.; Yamagata, K.; Katsura, K.-i.; Katayama, Y.; Asoh, S.; Ohta, S. Hydrogen acts as a therapeutic antioxidant by selectively reducing cytotoxic oxygen radicals. *Nature medicine* **2007**, *13*, 688.
- (11) Pshenichnyuk, S. A.; Komolov, A. S. Dissociative electron attachment to resveratrol as a likely pathway for generation of the H<sub>2</sub> antioxidant species inside mitochondria. *The journal of physical chemistry letters* **2015**, *6*, 1104–1110.
- (12) Pshenichnyuk, S. A.; Komolov, A. S. Dissociative electron attachment to anthralin to model its biochemical reactions. *The journal of physical chemistry letters* **2014**, *5*, 2916–2921.
- (13) Baur, J. A.; Sinclair, D. A. Therapeutic potential of resveratrol: the in vivo evidence. *Nature reviews Drug discovery* **2006**, *5*, 493.
- (14) de Oliveira, E. M.; Sanchez, S. d.; Bettega, M. H.; Natalense, A. P.; Lima, M. A.; Varella, M. T. d. N. Shape resonance spectra of lignin subunits. *Physical Review A* **2012**, *86*, 020701.
- (15) Szymańska, E.; Mason, N. J.; Krishnakumar, E.; Matias, C.; Mauracher, A.; Scheier, P.; Denifl, S. Dissociative electron attachment and dipolar dissociation in ethylene. *International Journal of Mass Spectrometry* **2014**, *365*, 356–364.

- (16) Arts, M. J.; Dallinga, J. S.; Voss, H.-P.; Haenen, G. R.; Bast, A. A critical appraisal of the use of the antioxidant capacity (TEAC) assay in defining optimal antioxidant structures. *Food Chemistry* **2003**, *80*, 409–414.
- (17) Ortega-Moo, C.; Garza, J.; Vargas, R. The substituent effect on the antioxidant capacity of catechols and resorcinols. *Theoretical chemistry accounts* **2016**, *135*, 1–12.
- (18) Frisch, M. J. et al. Gaussian09 Revision E.01. Gaussian Inc. Wallingford CT 2009.
- (19) Tsuzuki, S.; Honda, K.; Uchimaru, T.; Mikami, M.; Tanabe, K. Origin of attraction and directionality of the  $\pi/\pi$  interaction: model chemistry calculations of benzene dimer interaction. *Journal of the American Chemical Society* **2002**, *124*, 104–112.
- (20) Hwang, J.; Dial, B. E.; Li, P.; Kozik, M. E.; Smith, M. D.; Shimizu, K. D. How important are dispersion interactions to the strength of aromatic stacking interactions in solution? *Chemical Science* **2015**, *6*, 4358–4364.
- (21) Winstead, C.; McKoy, V. Interaction of low-energy electrons with the purine bases, nucleosides, and nucleotides of DNA. *The Journal of Chemical Physics* **2006**, *125*, 244302.
- (22) Dora, A.; Bryjko, L.; van Mourik, T.; Tennyson, J. Low-energy electron scattering with the purine bases of DNA/RNA using the R-matrix method. *The Journal of Chemical Physics* **2012**, *136*, 024324.
- (23) Nunes, F.; Varella, M.; Pastega, D. F.; Freitas, T.; Aurélio Pinheiro Lima, M.; Bettega, M.; Sanchez, S. Transient negative ion spectrum of the cytosine-guanine pair. *The European Physical Journal D* **2017**, *71*.
- (24) Scheer, A. M.; Burrow, P. D.  $\pi^*$  Orbital system of alternating phenyl and ethynyl groups: Measurements and calculations. *The Journal of Physical Chemistry B* **2006**, *110*, 17751–17756.
- (25) Santos, J. S. d.; da Costa, R. F.; Varella, M. T. d. N. Low-energy electron collisions with glycine. *The Journal of chemical physics* **2012**, *136*, 02B616.
- (26) Bettega, M.; Ferreira, L.; Lima, M. Transferability of local-density norm-conserving pseudopotentials to electron-molecule-collision calculations. *Physical Review A* **1993**, *47*, 1111.
- (27) da Costa, R. F.; Varella, M. T. d. N.; Bettega, M. H.; Lima, M. A. Recent advances in the application of the Schwinger multichannel method with pseudopotentials to electron-molecule collisions. *The European Physical Journal D* **2015**, *69*, 1–24.

- (28) Joachain, C. J. *Quantum collision theory*; 1975.
- (29) Bachelet, G.; Hamann, D.; Schlüter, M. Pseudopotentials that work: From H to Pu. *Physical Review B* **1982**, *26*, 4199.
- (30) Dunning Jr, T. H. Gaussian basis functions for use in molecular calculations. I. Contraction of (9s5p) atomic basis sets for the first-row atoms. *The Journal of Chemical Physics* **1970**, *53*, 2823–2833.
- (31) Ishimura, K.; McMurchie, L.; Davidson, E.; Rys, J. GAMESS-MW Schmidt, KK Baldrige, JA Boatz, ST Elbert, MS Gordon, JJ Jensen, S. Koseki, N. Matsunaga, KA Nguyen, S. Su, TL Windus, M. Dupuis, JA Montgomery J. Comput. Chem. 14, 1347-1363 (1993). *J. Comput. Chem* **1993**, *14*, 1347–1363.
- (32) Kossoski, F.; Bettega, M. Low-energy electron scattering from the aza-derivatives of pyrrole, furan, and thiophene. *The Journal of Chemical Physics* **2013**, *138*, 234311.
- (33) Bauschlicher Jr, C. W. The construction of modified virtual orbitals (MVO's) which are suited for configuration interaction calculations. *The Journal of Chemical Physics* **1980**, *72*, 880–885.
- (34) Roos, B. O.; Andersson, K.; Fülscher, M. P.; Serrano-Andrés, L.; Pierloot, K.; Merchán, M.; Molina, V. Applications of level shift corrected perturbation theory in electronic spectroscopy. *Journal of Molecular Structure: THEOCHEM* **1996**, *388*, 257–276.
- (35) Fdez. Galvan, I.; Vacher, M.; Alavi, A.; Angeli, C.; Aquilante, F.; Autschbach, J.; Bao, J. J.; Bokarev, S. I.; Bogdanov, N. A.; Carlson, R. K., et al. OpenMolcas: From source code to insight. *Journal of chemical theory and computation* **2019**, *15*, 5925–5964.
- (36) Curtiss, L. A.; Redfern, P. C.; Raghavachari, K. Gaussian-4 theory using reduced order perturbation theory. *The Journal of chemical physics* **2007**, *127*, 124105.
- (37) Cornetta, L.; Kossoski, F.; Varella, M. d. N. Transient anion spectra of the potential radiosensitizers 5-cyanateuracil and 5-thiocyanateuracil. *The Journal of Chemical Physics* **2017**, *147*, 214310.
- (38) Kossoski, F.; Bettega, M.; Varella, M. d. N. Shape resonance spectra of uracil, 5-fluorouracil, and 5-chlorouracil. *The Journal of chemical physics* **2014**, *140*, 024317.
- (39) Skurski, P.; Gutowski, M.; Simons, J. How to choose a one-electron basis set to reliably describe a dipole-bound anion. *International Journal of Quantum Chemistry* **2000**, *80*, 1024–1038.

- (40) Burrow, P.; Gallup, G. A.; Scheer, A. M.; Denifl, S.; Ptasinska, S.; Märk, T.; Scheier, P. Vibrational Feshbach resonances in uracil and thymine. *The Journal of chemical physics* **2006**, *124*, 124310.
- (41) Jordan, K.; Michejda, J.; Burrow, P. Electron transmission studies of the negative ion states of substituted benzenes in the gas phase. *Journal of the American Chemical Society* **1976**, *98*, 7189–7191.
- (42) Khatymov, R. V.; Muftakhov, M. V.; Mazunov, V. A. Phenol, chlorobenzene and chlorophenol isomers: resonant states and dissociative electron attachment. *Rapid communications in mass spectrometry* **2003**, *17*, 2327–2336.



**Supporting Information:**

**Low energy electron interactions with resveratrol  
and resorcinol: anion states and likely  
dissociation pathways**

Ely G. F. de Miranda,<sup>\*,†</sup> Lucas M. Cornetta,<sup>\*,‡</sup> and Márcio T. do N. Varella<sup>\*,†</sup>

*<sup>†</sup>Instituto de Física, Universidade de São Paulo, Rua do Matão 1371, 05508-090, São  
Paulo, São Paulo, Brazil*

*<sup>‡</sup>Instituto de Física Gleb Wataghin, Universidade Estadual de Campinas, Rua Sérgio  
Buarque de Holanda, 777 - Cidade Universitária, Campinas, São Paulo, Brazil*

E-mail: ely.miranda@usp.br; lucascor@unicamp.br; mvarella@if.usp.br

# Geometry optimization

The relative orientation of the two rings in t-RV significantly differs in the geometry optimizations performed with the B3LYP and  $\omega$ B97XD functionals, employing the 6-311++G(d,p) basis set in both cases. The optimal geometries are shown in Fig. S1 and Tab. S1, where the dihedral angles indicate a nearly planar structure for the B3LYP functional. The labels used in the dihedral angles are defined in Fig. S2. For the c-RV isomer, the geometries obtained with both functionals are similar (see Fig. S1).

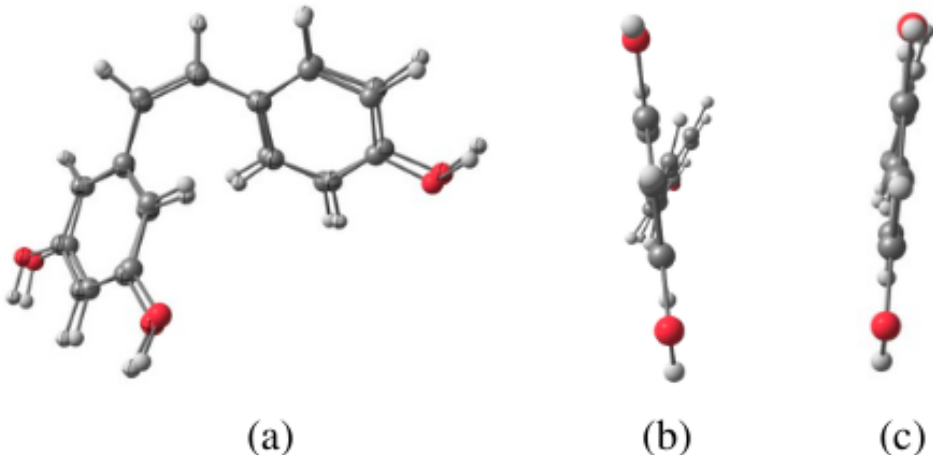


Figure S1: (a) Superimposed ground state geometries of the c-RV isomer optimized with the B3LYP and  $\omega$ B97XD functionals. The optimal geometries of the t-RV isomer obtained with the (b)  $\omega$ B97XD and (c) B3LYP functionals are also shown. All calculations employed the 6-311++G(d,p) basis set.

**Table S1: Dihedral angles (in  $^\circ$ ) for the t-RV isomer calculated with the  $\omega$ B97XD and B3LYP functionals. The atomic labels are given in Fig. S2.**

	$\omega$ B97XD	B3LYP
5-6-7-8	15.21	4.31
7-8-9-10	159.89	173.86
10-9-8-19	17.88	5.43
5-6-7-20	166.59	176.28

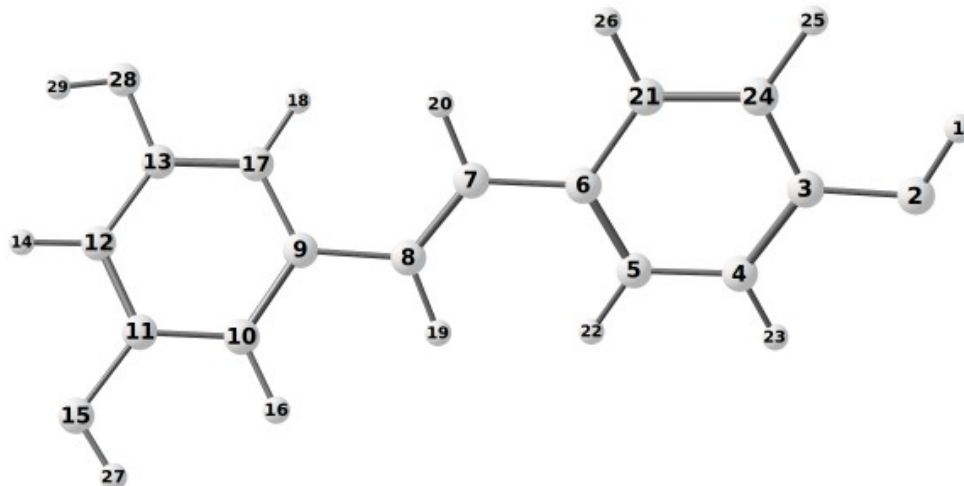


Figure S2: Atomic labels used in Tab. S1

## Excited states

The excitation spectra of the RS isomers were studied with the CASSCF/CASPT2 method and the ANO-L-VTZP basis set, employing the OpenMolcas software.<sup>S1</sup> These calculations can indicate the onset of electronic excitation in the scattering calculations and also possible parent states for core-excited resonances. The active space was built with 10 molecular orbitals. In the reference state, the 5 lowest-lying orbitals are doubly occupied and the remaining 5 orbitals are unoccupied. The molecular orbitals and their characters are indicated in Figs. S3 and S4 for the isomers (c) and (a), respectively (see the main text). Tab. S2 shows the results for the singlet and triplet states of both isomers. At least for the states considered here, the excitation energies are very close for the two conformers, with the lowest triplet states lying around 3.9 eV.

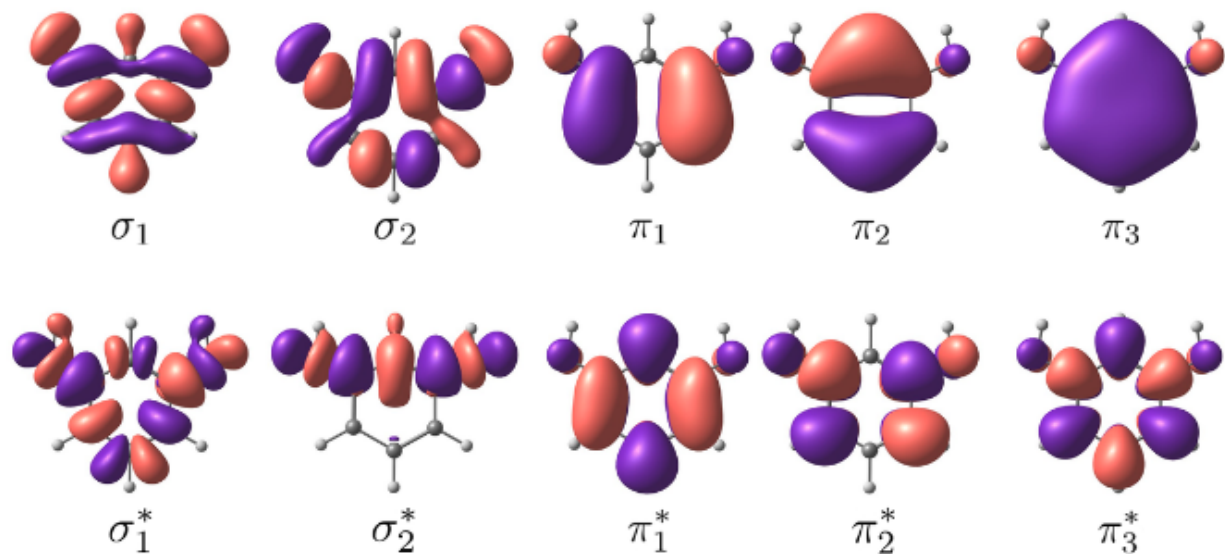


Figure S3: Molecular orbitals included in the active space of the CASSCF calculations performed for the (c) isomer of the RS molecule. In the reference state, the five upper orbitals were considered doubly occupied and the five lower orbitals unoccupied.

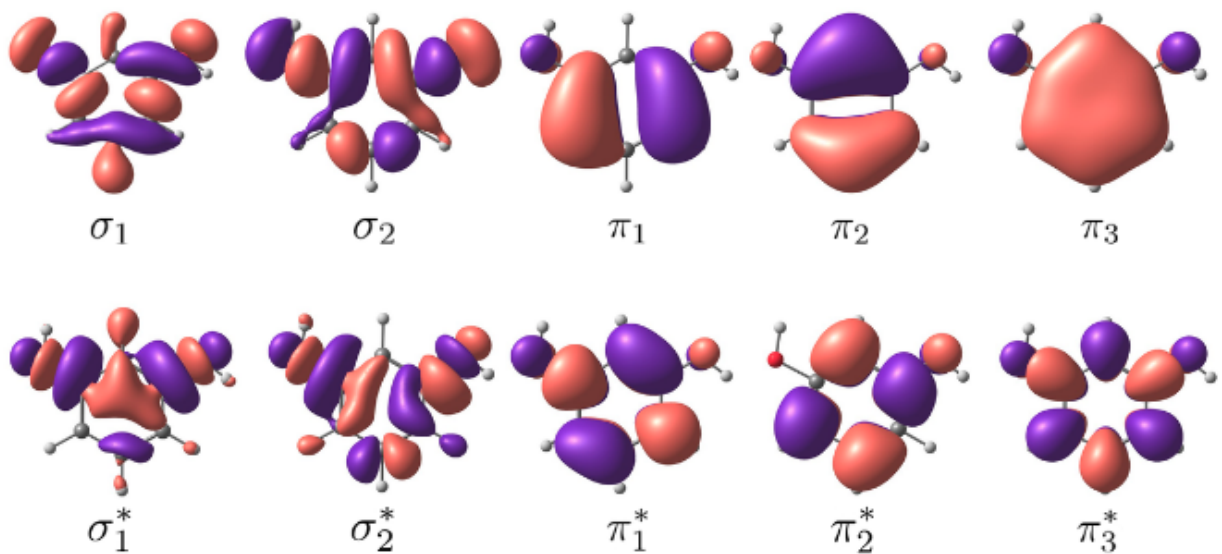


Figure S4: Molecular orbitals included in the active space of the CASSCF calculations performed for the (a) isomer of the RS molecule. In the reference state, the five upper orbitals were considered doubly occupied and the five lower orbitals unoccupied.

**Table S2:** Vertical excitation energies (in eV) for the (c) and (a) isomers of RS obtained with the CASPT2 method.

		(c)	(a)
Singlet	$1^1\pi\pi^*$	4.43	4.41
	$2^1\pi\pi^*$	5.66	5.47
	$3^1\pi\pi^*$	5.95	5.80
Triplet	$1^3\pi\pi^*$	3.92	3.89
	$2^3\pi\pi^*$	4.02	4.23
	$3^3\pi\pi^*$	4.49	4.42

## References

- (S1) Fdez. Galvan, I.; Vacher, M.; Alavi, A.; Angeli, C.; Aquilante, F.; Autschbach, J.; Bao, J. J.; Bokarev, S. I.; Bogdanov, N. A.; Carlson, R. K., et al. OpenMolcas: From source code to insight. *Journal of chemical theory and computation* **2019**, *15*, 5925–5964.